FUEL-EFFICIENT FLIGHT CONTROL DESIGN FOR A HYPERSONIC AIRLINER

Daniel Bodmer[1], Rhea Shah[1], Florian Linke[2] and Volker Gollnick[2]
[1]Hamburg University of Technology, Institute of Air Transportation Systems, Hamburg, Germany
[2]German Aerospace Center, Institute of Air Transportation Systems, Hamburg, Germany
e-mail: daniel.bodmer@tuhh.de, rhea.shah@tuhh.de, florian.linke@dlr.de and volker.gollnick@dlr.de

Abstract

The determination of realistic flight mission characteristics, such as fuel consumption and flight time, requires fuel-optimal flight trajectories where the vehicle's total trip fuel converges to a minimum. Within the *Stratospheric Flying Opportunities for High-Speed Propulsion Concepts* research project, one of the main challenging factors is the design of artificial flight controllers for maintaining 4D fuel-optimal trajectories for the STRATOFLY MR3 vehicle. In this paper, we propose a continuous climb cruise (CCC) flight controller as well as a zoom dive (ZD) flight controller which are derived using Feedback Linearization and embedded in a MATLAB-based trajectory simulation program. This incorporates the establishment of a proper control design model, an aircraft state estimator and the limitation of the plant's control inputs to ensure a bounded fast-time, forward integration of all aircraft state variables based on a 3 degrees of freedom point-mass model. Simulation results are presented showing that the CCC controller is primarily used in the hypersonic cruise phase – covering the main flight segment of MR3 – and that the ZD controller is used in the transonic region (while the vehicle reaches Mach 1), both ensuring a total decay of 2.98 % in the vehicle's fuel consumption for a reference flight mission from Brussels to Sydney.

Keywords

STRATOFLY, flight control, feedback linearization, trajectory simulation and optimization

DIRECTORIES

Abbreviations

ATC	Air Traffic Control
ATR	Air Turbo Rocket
CCC	Continuous Climb Cruise
CCO	Continuous Climb Operation
CDO	Continuous Descent Operation
DMR	Dual Mode Ramjet
DoF	Degrees of Freedom
ICA	Initial cruise altitude
LNAV	Lateral Navigation
MIL	Model-in-the-loop
ROCD	Rate of Climb or Descent
TAS	True Airspeed
TCM	Trajectory Calculation Module
VNAV	Vertical Navigation
ZD	Zoom Dive

List of Symbols

$C_{l,cruise}$	Lift coefficient during cruise flight
$\dot{C}_{l,cruise}$	Change of $C_{l,cruise}$ over time
D	Drag force
e	Tracking error
$\boldsymbol{e}$	Tracking error vector
E_S	Specific energy level
$\dot{E}_S$	Change of E_S over time
$\overline{FF}$	Average fuel flow
g	Gravitational acceleration
h	True altitude
h_{CFA}	Cruise flight altitude
$\dot{h}$	Rate of climb or descent
$\tilde{\dot{h}}$	Pseudo control
k	Feedback gain
L	Lift force
m	Mass
$\dot{m}$	Change of mass over time
S	Wing reference area
T	Thrust force
T_{max}	Maximum thrust force
T_{min}	Minimum thrust force
$\tilde{T}$	Pseudo control
$\boldsymbol{u}$	Plant input vector
$\tilde{\boldsymbol{u}}$	Controller output vector
V_{TAS}	True airspeed
$\dot{V}$	Absolute acceleration
$\tilde{\dot{V}}$	Pseudo control
x_I	Axis of inertial frame in x-direction
$\boldsymbol{y}$	Plant output vector
z_I	Axis of inertial frame in z-direction
γ	Climb path angle
γ_c	Commanded climb path angle
Θ	Longitudinal tilt angle
Φ	Bank angle
ρ	Atmospheric density
$\dot{\rho}$	Change of atmospheric density over time

doi: 10.25967/550184

Operators

$\|\cdot\|$	Euclidean norm of a vector
$(\cdot)^2$	raised to the power of 2
$(\cdot)^3$	raised to the power of 3

1. INTRODUCTION

Hypersonic air travel has been a topic of extensive research for years now [1]-[5] since the extension of hypersonic technologies to civil aviation can substantially reduce the duration of, e.g., antipodal flights. Relating thereto, the Stratospheric Flying Opportunities for High-Speed Propulsion Concepts (STRATOFLY) research project was set up in 2018 to investigate the feasibility of high-speed passenger stratospheric flights with respect to key technological, societal, and economical aspects ([6]). A hypersonic aircraft concept, the STRATOFLY MR3, was designed to fly at cruise speed of Mach 8 and at altitudes above 30km i.e. in the stratosphere. LAPCAT MR2.4 [7], which was derived by means of an iterative design process to achieve structural integrity, improved volume efficiency and optimal airframe-propulsion integration with an elliptical air intake, serves as the baseline for this new vehicle design. Both vehicles are equipped with a hydrogen-based propulsive system consisting of six Air Turbo Rockets (ATRs), being used for a Mach range from 0 to 4, and one Dual Mode Ramjet (DMR), to power the vehicle up from Mach 4 to 8. The MR3 vehicle maintains the external waverider configuration of the MR2.4 vehicle, however, structural design, propulsion or aerodynamics including, e.g., empennages or flight control surfaces have been improved. ([8]-[11])

FIG. 1: STRATOFLY-MR3 vehicle concept [6]

1.1. Literature Overview

Within the scope of the STRATOFLY research project, one of the most challenging factors is the design of fuel-optimal flight trajectories where the vehicle's trip fuel is reduced to a minimum while simultaneously meeting the overall constraints prescribed by the Air Traffic Control (ATC). The vehicle's performance strongly depends on its propulsive and aerodynamic efficiency which requires robust flight controllers for maintaining fuel-optimal design points over the entire operating profile. We call these flight controllers *fuel-efficient* in the scope of trajectory modeling and optimization.

Integration of continuous climb operations (CCOs) and continuous descent operations (CDOs) has been identified as a promising approach to optimize flight trajectories to reduce the fuel consumption over the course of a flight ([12], [13]). In comparison to the conventional climb profiles, the benefits of CCOs and CDOs are established by waiving of the level off segments, whereby noise and inefficient acceleration phases are avoided and intermediate altitude clearances during climb are no longer applied ([13]). Several studies such as [14]-[16] have assessed the benefits of employing continuous operations over conventional procedures for commercial aircraft. These works, however, are focused on current commercial aircraft, which solely comprise of flights in the subsonic regime. The vertical flight profile of STRATOFLY MR3, the focus vehicle in this study, is designed largely to be continuous by extending the concept of CCOs (within the climb and cruise phase) to supersonic and hypersonic regimes to assure its proximity to the optimal solution.

The state of the art in trajectory optimization of hypersonic air breathing vehicles comprises of a number of direct and indirect techniques. E.g. [17] uses gauss pseudo spectral method to optimize hypersonic vehicle trajectories by discretizing a continuous control problem into Legendre-gauss points. [18] proposes an inverse dynamic approach for solving the ascent problem for an aerospace plane whereas [19] presents an optimal control problem employing nonlinear programming and collocation method to derive for e.g. minimum-time climb trajectories. [20] is a pioneering work that inferred the total energy to be a significant quantity in performance analysis of high-speed aircraft. Relating thereto, [21] simplified the aircraft dynamics to a point mass energy approximation model being used in performance optimization of a supersonic aircraft. [22] extends the energy approximation methods for flight performance optimization in terms of minimum-time climbs trajectories by applying singular perturbation methods to take the fast dynamics of fighter aircrafts into account. [23] further addresses whether energy state method is an appropriate method to obtain optimal flight trajectories in terms of scramjet-powered hypersonic vehicles. Based on these results, it can be concluded that the use of energy-state approximation is a justified and widely accepted assumption for this class of vehicles.
The climb profile of STRATOFLY MR3 is therefore optimized by adapting the concept of energy methods to trajectory modeling and optimization. Based on the optimal flight profiles obtained in [20] and [21], a detailed assessment of the flight when the aircraft approaches Mach 1 is conducted and a specific energy dive or rather zoom dive (ZD) flight controller is implemented for the transonic regime which is in the spirit of the stated findings in literature.

Considerable amount of research has been undertaken on hypersonic cruise trajectory optimization due to the potential the cruise phase offers in fuel saving. Most studies focus on optimal periodic cruise solutions for hypersonic vehicles. [24]-[27] assess the fuel reduction achieved with the utilization of periodic cruise trajectories over steady state trajectories using various numerical methods. E.g. [27] attempts to realize periodic hypersonic cruise by maintaining the lift coefficient and velocity constant to investigate the effects on aerodynamic heating and fuel performance. In contrast to these efforts, optimal cruise flight conditions for MR3 are derived by evaluating the extension of continuous climb cruise (CCC) operations to the hypersonic regime. Available resources pertaining to this approach are quite limited. To optimize the cruise profile by adapting the CCC technique, the *Breguet range equation* [28] can be maximized (minimized fuel) by

maximizing the influencing parameters such as, e.g., the lift-to drag ratio. Premised on this fact, MR3 cruise trajectory is designed to follow the constant lift coefficient and constant Mach number cruise flight program, which allows the selection of an optimal lift coefficient. The conclusion obtained in [27] that the lift coefficient could be recognized as a constant and thus be optimized is favorable to the approach adapted here, in this paper.

The design of adequate flight controllers plays a key role in realizing fuel-optimal trajectories and consequently facilitates making air breathing hypersonic flights more feasible. Fuel-optimal flight controllers and correlated approaches have been investigated for years now leading to development of various methodologies [29]-[32]. [30], e.g., applies energy state approximation for a 3 degrees of freedom (DoF) transatmospheric vehicle model. Feedback laws are derived using a combination of singular perturbation and feedback linearization techniques. This analysis and [29], [31], [32] prove feedback linearization to be a superior technique for deriving feedback laws while using energy state approximation in 3 DoF closed-loop control systems.
Relating thereto, early studies on the use of energy-based approaches were focused on the performance of fighter aircraft. For e.g., [33] describes guidance algorithms for a 6 DoF rigid-body model of an F-15 aircraft for fast transitions. The algorithm is based on total energy control principle to regulate total energy state and flight path angle using throttle for fast vertical state transition. STRATOFLY MR3 is intended for commercial use and fast vertical transitions are avoided as passenger comfort takes precedence. However, the specific energy hold controller developed in [33] has clearly inspired the idea of deriving the ZD flight controller in this paper. Similar to the energy hold throttle control law in [33], control laws for a specific energy dive are derived using feedback linearization techniques.
Due to the lack of available resources on the derivation of flight controllers being used for constant lift coefficient and constant Mach number cruise flight programs only [27] was identified to be relevant in the scope of designing fuel-optimal hypersonic trajectories. Here, thrust and lift coefficients are derived analytically based on optimal Hamiltonian control theory to encounter high fuel efficient and low aerodynamic heated trajectories for a simplified open-loop dynamic model. Since the derivation of stable closed-loop control laws is not included in [27], a CCC flight controller (for maintaining a constant lift coefficient during the hypersonic cruise phase) is derived in this paper, analogous to the ZD controller, using feedback linearization technique for a nonlinear control design model.

1.2. Objective, Scope and Outline

The main objective of this paper is to present appropriate control laws derived using feedback linearization technique, to design fuel-optimal flight trajectories for the hypersonic vehicle STRATOFLY MR3. Applying energy methods in the supersonic climb phase as well as CCC operations in the hypersonic cruise phase, two *fuel-efficient* flight controllers are embedded in a 4D-trajectory simulation program. The control laws are derived analytically which incorporates the establishment of a proper control design model, an aircraft state estimator and the limitation of the plant's control inputs within the 3 DoF closed-loop control system.
The paper is organized as follows: It starts with a brief introduction of the 4D-trajectory simulation software in section 2 followed by a detailed derivation of the fuel-efficient flight controllers in section 3. Section 4 presents simulation results for both controllers and Section 5 concludes the paper with a brief summary and future work potential.

2. TRAJECTORY CALCULATION MODULE

The Trajectory Calculation Module (TCM) is a MATLAB-based mission simulator to calculate 4D flight trajectories. The tool was originally developed by DLR's Institute of Air Transportation Systems [34] and provides a fast-time, forward integration of aircraft state variables based on simplified point-mass equations of motion. Depending on the flight mission and user preferences, *high-level* and *low-level* convergence criteria are defined by tolerances in the internal tool structure to check to what extent the exit condition of the particular flight segment (e.g. speed and altitude schedule) has been reached. Furthermore, the aircraft's cruise phase distance is iteratively adjusted until the top of descent is re-shifted so that the destination airport is reached within the set of permissible deviations (vertical=altitude and lateral=distance). Since TCM provides an adjustable interface for aircraft performance data to generate engine and aerodynamic lookup tables, it is possible to calculate flight movements of a variety of aircraft types. In the scope of STRATOFLY, TCM was adapted and extended with the aerodynamic and propulsive databases of MR3 to meet the project requirements. Further information on this can be found in [11] and [35]-[38].

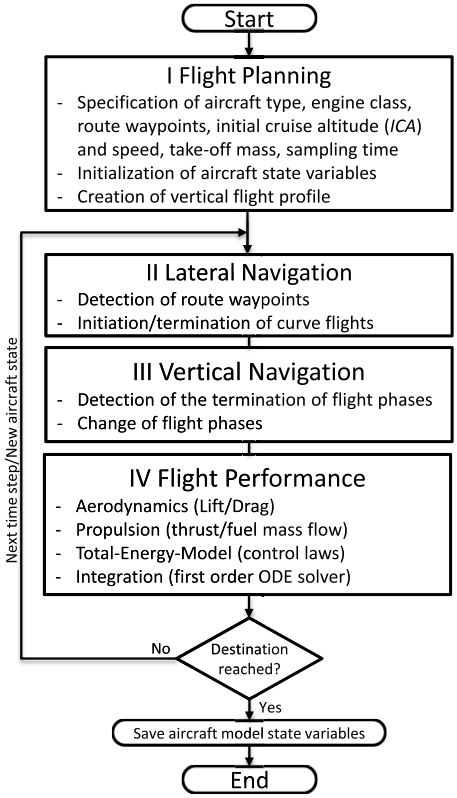

FIG. 2: Program flow of Trajectory Calculation Module (based on [34])

The program flow of TCM is divided into four functional main blocks as shown in FIG. 2. In the first block, a flight phase table including target and exit conditions of each individual flight segment is generated and the aircraft model state variables are initialized to the corresponding start values. This is followed by the execution of the primary simulation loop which comprises of the three main blocks, blocks II to IV. In terms of the lateral navigation (LNAV), the reaching of waypoints is detected and, if necessary, curve flights are initiated and terminated based on the current position of the aircraft. During the vertical navigation (VNAV), which corresponds to the third main block, the simulation module checks whether flight conditions that terminate the current flight phase have been reached or not. If the conditions have been met, the program routine switches to the subsequent flight phase. In the last block, flight performance calculations are performed, aerodynamic and engine models are evaluated, and the desired aircraft movement is obtained by calculating the control laws based on the Total-Energy-Model [39]. The new aircraft states are determined by integrating the current state variables numerically over time using Euler's method [40]. This forms the starting point for the next run of the primary simulation loop, which is executed until the entire target flight profile has been completed. Finally, the results of the TCM simulation are stored. For further information and theoretical basics of the tool, please refer to [41] and [42].

3. CONTROLLER DESIGN

The calculation of operationally realistic flight trajectories in the preliminary design phase of a conceptual vehicle such as STRATOLFY MR3, involves the design of artificial flight controllers extending the conventional classification of the aircraft's lateral, longitudinal, or directional control to satisfy a fuel-optimized flight envelope ([43]).
In this section, we propose a CCC flight controller as well as a ZD flight controller that aim to reduce the aircraft's fuel consumption in order to address the environmental strain of hypersonic air transport systems. The CCC controller is primary used in the hypersonic cruise phase to perform a constant lift coefficient and constant Mach number cruise flight program avoiding intermediate level-off segments. The ZD flight controller is used during the climb phase in the transonic region while the aircraft reaches Mach 1. Both controllers are based on *Feedback Linearization* [44] which is, in general, used to make a dynamic system or rather its state trajectory follow a desired reference trajectory by determining an appropriate control law. This control law tries to cancel out the aircraft's inherent dynamics in order to replace them with desired linear dynamics to be tracked by the corresponding aircraft states. FIG. 3 shows TCM's closed-loop control system where the *plant* is represented by a 3 DoF point mass model of STRATOFLY MR3. The controller output vector $\tilde{\boldsymbol{u}} \in \mathbb{R}^3$ contains the aircraft's desired virtual controls which are transformed to the physically attainable set of the aircraft's system inputs $\boldsymbol{u} \in \mathbb{R}^3$ based on MR3's engine performance model. Since the overall TCM testbed is treated as a model-in-the-loop (MIL) simulation, the controller states are initialized through the plant's output vector $\boldsymbol{y}$ and a state estimator model is embedded to not only define the tracking errors for the ZD and CCC flight controller, but also to artificially provide quantities which are not comprised in the plant's output vector $\boldsymbol{y}$ from scratch.

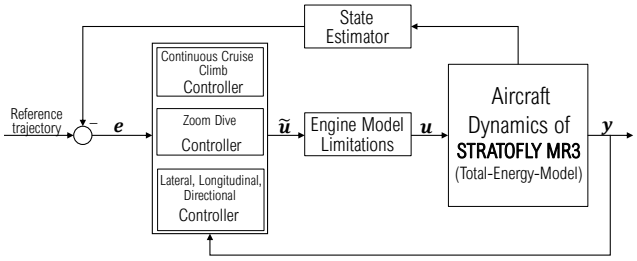

FIG. 3: Illustration of TCM's closed-loop control system (based on [41], [43])

3.1. Control Design Model

In control theory, a simplified mathematical description of the plant is used, in general, as control design model which only takes aspects and properties of physical significance into account to derive the control laws from scratch. Since the aircraft dynamics in the TCM is based on the Total-Energy-Model [39], this model description is likewise used as nonlinear control design model to derive the feedback laws for the CCC and ZD flight controller. As shown in FIG. 3, all state variables are initialized through the plant output vector $\boldsymbol{y}$.
In the Total-Energy-Model, the aircraft is simplified as a 3 DoF point mass where the thrust force T and the drag force D are both parallel and the lift force L is perpendicular to the true airspeed V_{TAS}. By assuming that Earth is non-rotating and flat, without any elliptical shape, we can apply *Newton's 2nd law of motion* [40] in the direction of V_{TAS} which yields

$$m \cdot \dot{V} = T - D - m \cdot g \cdot \sin(\gamma), \tag{1}$$

where m denotes the aircraft's mass, g the gravitational acceleration, γ the climb path angle and $\dot{V}$ the absolute acceleration which is the time derivative of the aircraft's true airspeed V_{TAS} with respect to an inertial (*I*) reference frame being located at the Earth's surface. The *I*-frame has a non-relocatable placement at the aircraft's point of departure. Its x-y plane is parallel and its z_I-axis is perpendicular to the local surface whereby the x_I-axis points to the geographic north pole. For the rate of climb or descent (ROCD), the kinematic relation

$$\dot{h} = V_{TAS} \cdot \sin(\gamma), \tag{2}$$

holds, where $\dot{h}$ denotes the time derivative of the aircraft's true altitude h with respect to the *I*-frame. By solving eq. (2) for $\sin(\gamma)$ and then inserting it into eq. (1), we finally obtain the standard formulation of the Total-Energy-Model:

$$(T - D) \cdot V_{TAS} = m \cdot g \cdot \dot{h} + m \cdot V_{TAS} \cdot \dot{V} \tag{3}$$

Physically, eq. (3) can be interpreted as a power balance, where the excess power is equal to the sum of potential and kinetic energy, respectively, their correlated changes over time. By neglecting the aircraft's high-lift devices as well as spoilers, the longitudinal aircraft movement is mainly controlled by the elevator deflection and the thrust force. Thus, through appropriate pseudo control laws for $\tilde{T} \in \tilde{\boldsymbol{u}}$ and $\dot{\tilde{h}} \in \tilde{\boldsymbol{u}}$, which are transformed into physical plant inputs $T \in \boldsymbol{u}$ and $\dot{h} \in \boldsymbol{u}$ by actuator limitations (see section 3.5), two of the three plant inputs are already defined so that the third quantity can be obtained through a conservation of energy on the basis of eq. (3).

3.2. State Estimator

A state estimator is embedded into the closed-loop control system of TCM to not only define the tracking errors for the ZD and CCC flight controller, but also to artificially provide quantities which are not comprised in the plant's output vector $\boldsymbol{y}$ from scratch (see FIG. 3). The estimation algorithms are repeated for every time instance Δt, which also defines the sampling time increments of TCM ensuring synchronous interactions and timing.
For the ZD controller, the aircraft's specific energy level as well as its time derivative with respect to the *I*-frame are determined by ([21])

$$E_S = h + \frac{V_{TAS}^2}{2 \cdot g}, \tag{4}$$

$$\dot{E}_S = \dot{h} + \frac{V_{TAS}}{g}\dot{V} = \frac{(T - D) \cdot V_{TAS}}{m \cdot g}. \tag{5}$$

In addition to the CCC flight controller, a vertical balance of forces leads to an analytical formulation for the aircraft's lift coefficient during cruise flight, where it is assumed, that the aircraft's longitudinal tilt angle Θ is always small and therefore neglectable:

$$C_{l,cruise} = \frac{2 \cdot m \cdot g}{\rho \cdot V_{TAS}^2 \cdot S \cdot \cos(\Phi)}. \tag{6}$$

In eq. (6), ρ denotes the aircraft's surrounding atmospheric density, S the wing reference area, and Φ the aircraft's bank angle which is assumed to be negligibly small for the cruising flight segment. The general formula for the derivation of the lift coefficient with respect to the *I*-frame can, based on eq. (6), be written as follows

$$\dot{C}_{l,cruise} = \frac{dC_{l,cruise}}{dV_{TAS}}\dot{V} + \frac{dC_{l,cruise}}{dm}\dot{m} + \frac{dC_{l,cruise}}{d\rho}\dot{\rho}, \tag{7}$$

where $\dot{m}$ denotes the time derivative of the aircraft's total mass as well as $\dot{\rho}$ denotes the time derivative of the atmospheric density. Applying Euler's classical treatment of vector analysis [40], we calculate the partial differentials in eq. (7) by deriving eq. (6) with respect to V_{TAS}, m and ρ leading to

$$\dot{C}_{l,cruise} = -\frac{4 \cdot m \cdot g}{\rho \cdot S \cdot V_{TAS}^3}\dot{V} + \frac{2 \cdot g}{\rho \cdot S \cdot V_{TAS}^2}\dot{m} - \frac{2 \cdot m \cdot g}{\rho^2 \cdot S \cdot V_{TAS}^2}\dot{\rho}. \tag{8}$$

To solve eq. (8), we firstly assume a linear decrease of the aircraft's mass over time which is directly proportional to the engine's average fuel flow $\overline{FF}$. An estimation of the aircraft's fuel flow consumption can be made by evaluating MR3's engine property database for cruise conditions which yields $\overline{FF} = 9\ \mathrm{m/s}$. Secondly, we assume that the standard ICAO atmospheric conditions [45] hold during cruise so that the change of density over time is given by

$$\dot{\rho} = -1.4276 \cdot 10^{-5} \cdot [1 + 4.5425 \cdot 10^{-6}(h_{ICA} - 20000)]^{-36.7143} \cdot \dot{h} \tag{9}$$

for altitudes above $20000\ \mathrm{m}$. Since the initial cruise altitude (ICA) forms a user input of TCM (see FIG. 2), h_{ICA} in eq. (9) is predefined. After substituting the analytical formulation of the lift coefficient so that $C_{l,cruise}$ is explicitly included, eq. (8) can be rewritten to

$$\dot{C}_{l,cruise} = -\frac{2 \cdot C_{l,cruise}}{V_{TAS}}\dot{V} - \frac{C_{l,cruise}}{m}\overline{FF} + \frac{C_{l,cruise}}{\rho}\{1.4276 \cdot 10^{-5} \cdot [1 + 4.5425 \cdot 10^{-6}(h_{ICA} - 20000)]^{-36.7143} \cdot \dot{h}\}. \tag{10}$$

3.3. Zoom Dive Flight Controller

To derive the control law for the ZD flight controller, 1st order energy error dynamics are stabilized by the pseudo controls $\tilde{T}, \dot{\tilde{h}}$ and $\dot{\tilde{V}}$ around their zero equilibrium. The control objective has been reached when the specific energy level E_S tracks a desired reference trajectory $E_{S,r}$ so that the specific energy level tracking error e_{ZD} and its time derivative converge to zero:

$$e_{ZD} = E_S - E_{S,r} \tag{11}$$

$$\dot{e}_{ZD} = \dot{E}_S - \dot{E}_{S,r} \tag{12}$$

First, we rewrite the energy error dynamics by inserting eq. (5) into eq. (12) which yields

$$\dot{e}_{ZD} = \frac{(T - D) \cdot V_{TAS}}{m \cdot g} - \dot{E}_{S,r} \tag{13}$$

Note that a linear reference model, as e.g. a PT1 filter [46], shall be used to generate the feasible reference trajectories for the ZD controller. However, since it is the controller's purpose to maintain a constant specific energy level during the dive, we command a predefined optimal specific energy level so that the desired reference trajectory $E_{S,r}$ remains in a steady-state which yields $\dot{E}_{S,r}$ being equal to zero. Next, assume that the pseudo control $\tilde{T}$ does establish

$$\dot{e}_{ZD,d} = -k_{p,ZD} \cdot e_{ZD} - k_{i,ZD} \cdot \left[\int_{t_0}^{t} (e_{ZD})\, dt\right], \tag{14}$$

which denotes a desired decay behavior of the real specific energy level error dynamics $\dot{e}_{ZD}$. Both feedback gains $k_{p,ZD}$ and $k_{i,ZD}$ are Hurwitz and of the set $\mathbb{R}^{1x1}$. If the aircraft's total thrust $T \in \boldsymbol{u}$ is selected according to the pseudo control law

$$\tilde{T} = \frac{\dot{e}_{ZD,d} \cdot m \cdot g}{V_{TAS}} + D, \tag{15}$$

the desired error dynamics in eq. (14) and the real error dynamics in eq. (13) become equal so that the specific energy level E_S approaches its reference trajectory $E_{S,r}$ exponentially fast. Note that by using eq. (2), we have another parametric quantity of how the interrelated conversion rate between kinetic and potential energy in eq. (3) is weighted. That is why we command a constant desired climb path angle γ_c of -3° to constitute the pseudo control law

$$\dot{\tilde{h}} = V_{TAS} \cdot \sin(\gamma_c), \tag{16}$$

which is then used, together with $\tilde{T}$, to determine $\dot{\tilde{V}}$ by inserting eq. (15) and (16) into eq. (3) yielding

$$\dot{\tilde{V}} = \frac{(\tilde{T} - D)}{m} - \frac{g \cdot \dot{\tilde{h}}}{V_{TAS}}. \tag{17}$$

For the sake of completeness, we can finally provide the solution of the ZD controller architecture in the Laplace domain by inserting the pseudo controls, given by eq. (15)-(17), into the specific energy kinematics, given by eq. (5), which yields

$$\dot{\tilde{E}}_S = \dot{\tilde{h}} + \frac{V_{TAS}}{g}\dot{\tilde{V}} = -k_{p,ZD} \cdot e_{ZD} - k_{i,ZD} \cdot \left[\int_{t_0}^{t} (e_{ZD})\, dt\right]. \tag{18}$$

Note that eq. (18) cannot be considered explicitly as pseudo control law since the specific energy level or rather its time derivative are solely provided by the state estimator (see FIG. 3) and therefore excluded from the

plant's aircraft dynamics. However, for illustration purposes, FIG. 4 manifests that a linear PI-controller stabilizes the specific energy level tracking error, respectively, its time derivative to obtain asymptotic tracking of E_S and $E_{S,r}$.

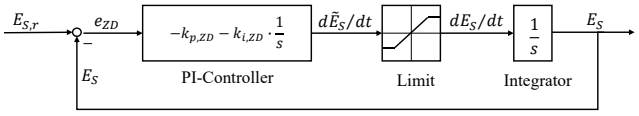

FIG. 4: Zoom dive flight controller architecture

3.4. Continuous Cruise Climb Flight Controller

The purpose of the CCC flight controller is that the aircraft performs a constant lift coefficient and constant true airspeed cruise flight program. Thus, to derive the control laws for the CCC controller, we stabilize 1st order velocity error dynamics as well as 1st order lift coefficient error dynamics by the pseudo controls $\tilde{T}, \tilde{\dot{h}}$ and $\tilde{\dot{V}}$ around their zero equilibria. The control objectives have been reached when V_{TAS} tracks a desired reference trajectory $V_{TAS,r}$ as well as when C_l tracks a desired reference trajectory $C_{l,r}$ so that the tracking error

$$\boldsymbol{e}_{CCC} = \begin{pmatrix} e_{TAS} \\ e_{C_l} \end{pmatrix} = \begin{pmatrix} V_{TAS} - V_{TAS,r} \\ C_{l,cruise} - C_{l,r} \end{pmatrix} \in \mathbb{R}^2 \tag{19}$$

as well as its time derivative

$$\dot{\boldsymbol{e}}_{CCC} = \begin{pmatrix} \dot{e}_{TAS} \\ \dot{e}_{C_l} \end{pmatrix} = \begin{pmatrix} \dot{V} - \dot{V}_r \\ \dot{C}_{l,cruise} - \dot{C}_{l,r} \end{pmatrix} \in \mathbb{R}^2, \tag{20}$$

converge to zero. First, in terms of the aircraft's velocity control, assume that the pseudo control $\tilde{V}$ does establish

$$\dot{e}_{TAS,d} = -k_{p,TAS} \cdot e_{TAS} - k_{i,TAS} \cdot \left[\int_{t_0}^{t} (e_{TAS})\, dt \right], \tag{21}$$

which denotes a desired decay behavior of the real velocity error dynamics $\dot{e}_{TAS} = (1 \;\; 0)\dot{\boldsymbol{e}}_{CCC}$. Both feedback gains $k_{p,TAS}$ and $k_{i,TAS}$ are constant and Hurwitz. If the aircraft's absolute acceleration $\dot{V} \in \boldsymbol{u}$ is selected according to the pseudo control law

$$\tilde{\dot{V}} = \dot{V}_r - k_{p,TAS} \cdot e_{TAS} - k_{i,TAS} \cdot \left[\int_{t_0}^{t} (e_{TAS})\, dt \right], \tag{22}$$

the desired velocity error dynamics in eq. (21) and the real velocity error dynamics in (22) become equal so that V_{TAS} approaches its reference trajectory $V_{TAS,r}$ exponentially fast. Note that since we want to maintain a constant predefined airspeed during the entire cruise flight segment, our desired reference trajectory $V_{TAS,r}$ remains in a steady-state which yields $\dot{V}_r$ being equal to zero as adequate simplification in our control law.

Secondly, in terms of the aircraft's lift control, we insert the estimated lift coefficient dynamics, given by eq. (10), into eq. (20) and extract the 1st order C_l-error dynamics by $\dot{e}_{C_l} = (0 \;\; 1)\dot{\boldsymbol{e}}_{CCC}$ which yields

$$\begin{aligned} \dot{e}_{C_l} = &-\frac{2 \cdot C_{l,cruise}}{V_{TAS}} \tilde{\dot{V}} - \frac{C_{l,cruise}}{m} \overline{FF} \\ &+ \frac{C_{l,cruise}}{\rho} \{1.4276 \cdot 10^{-5} \cdot [1 \\ &+ 4.5425 \cdot 10^{-6} (h_{ICA} - 20000)]^{-36.7143} \cdot \dot{h}\} - \dot{C}_{l,r}. \end{aligned} \tag{23}$$

To ensure that asymptotic velocity tracking is guaranteed while stabilizing the C_l-error dynamics, we use the pseudo control law $\tilde{\dot{V}}$ in eq. (23). Furthermore, let

$$\dot{e}_{C_l,d} = -k_{p,C_l} \cdot e_{C_l} - k_{i,C_l} \cdot \left[\int_{t_0}^{t} (e_{C_l})\, dt \right], \tag{24}$$

denote a desired decay behavior of the real lift coefficient error dynamics $\dot{e}_{C_l}$, where k_{p,C_l} and k_{i,C_l} are Hurwitz feedback gains of the set $\mathbb{R}^{1x1}$. Assume that $\dot{e}_{C_l,d}$ can be generated by a desired pseudo control input $\tilde{\dot{h}}$ so that in case the aircraft's ROCD $\dot{h} \in \boldsymbol{u}$ is selected according to $\tilde{\dot{h}}$, the desired error dynamics (24) and the real error dynamics (23) become equal. Thus, after a comparison of coefficients, we find the pseudo control law

$$\begin{aligned} \tilde{\dot{h}} = k_{C_l} \Bigg[&\dot{C}_{l,r} - k_{p,C_l} \cdot e_{C_l} - k_{i,C_l} \cdot \left[\int_{t_0}^{t} (e_{C_l})\, dt \right] \\ &+ \frac{2 \cdot C_{l,cruise}}{V_{TAS}} \tilde{\dot{V}} + \frac{C_{l,cruise}}{m} \overline{FF} \Bigg], \end{aligned} \tag{25}$$

with

$$k_{C_l} = \frac{\rho}{1.4276 \cdot 10^{-5} \cdot [1 + 4.5425 \cdot 10^{-6} (h_{ICA} - 20000)]^{-36.7143} \cdot C_{l,cruise}} \in \mathbb{R}. \tag{26}$$

Since the controller's key purpose is to maintain a constant lift coefficient during the CCC operation, we command a predefined initial lift coefficient so that the desired reference trajectory $C_{l,r}$ remains in a steady-state which yields $\dot{C}_{l,r}$ being equal to zero as adequate simplification. With regard to the conservation of energy within our control design model (see section 3.1), we derive the pseudo control law $\tilde{T}$ by inserting eq. (22) and (25) into eq. (3) yielding

$$\tilde{T} = \frac{m \cdot g}{V_{TAS}} \cdot \tilde{\dot{h}} + m \cdot \tilde{\dot{V}} + D. \tag{27}$$

If the aircraft's absolute acceleration, ROCD and total thrust are selected according to their pseudo control laws $\tilde{\dot{V}}$, $\tilde{\dot{h}}$ and $\tilde{T}$, the Euclidean norm $\|\boldsymbol{e}_{CCC}\|_2$ converges to zero so that the aircraft's true airspeed V_{TAS} and the lift coefficient C_l approach their reference trajectories exponentially fast. For the sake of completeness, we divide the CCC flight controller in two parts, a V_{TAS}-based velocity controller and a C_l-based lift coefficient controller, to depict their architectures in the Laplace domain. For the aircraft's velocity control, on the basis of eq. (22), FIG. 5 manifests that a linear PI-controller stabilizes the true airspeed tracking error, respectively, its time derivative to obtain asymptotic tracking of V_{TAS} and $V_{TAS,r}$.

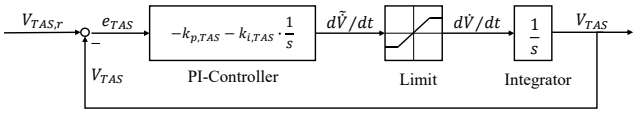

FIG. 5: Continuous cruise climb flight controller – V_{TAS} control architecture

For the C_l-based lift coefficient controller, we provide its architecture in the Laplace domain by inserting $\tilde{\dot{h}}$, given by eq. (25) and (26), into the lift coefficient kinematics, given by eq. (10), which yields

$$\dot{\tilde{C}}_{l,cruise} = -k_{p,C_l} \cdot e_{C_l} - k_{i,C_l} \cdot \left[\int_{t_0}^{t} (e_{C_l})\, dt \right]. \tag{28}$$

Note that eq. (28) cannot be considered explicitly as pseudo control law since the lift coefficient or rather its time derivative are solely provided by the state estimator (see section 3.2), not contributing to the plant inputs of the

closed-loop control system. However, for illustration purposes, FIG. 6 manifests that a linear PI-controller stabilizes the lift coefficient tracking error, respectively, its time derivative to obtain asymptotic tracking of $C_{l,cruise}$ and $C_{l,r}$.

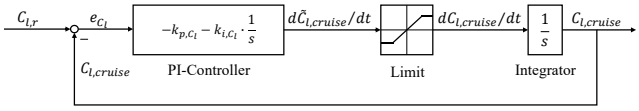

FIG. 5: Continuous cruise climb flight controller – C_l control architecture

3.5. Limitation of Pseudo Control Inputs

In the closed-loop control system of TCM a limitation of the pseudo control inputs $\tilde{V}$, $\tilde{\dot{h}}$ and $\tilde{T}$ is necessary to transform them into valid system inputs $\dot{V}$, $\dot{h}$ and T which are contributing to the system input vector $\boldsymbol{u}$. Since $\tilde{V}$, $\tilde{\dot{h}}$ and $\tilde{T}$ can directly be manipulated by the inputs of the system, or rather, become valid inputs after their limitation, they were considered as pseudo controls in the previous sections. For clarity, if it can be found that the pseudo control inputs are within their permitted range for every time instance Δt of the simulation, the word *pseudo* becomes meaningless and the control laws, derived in section 3.3 and 3.4, hold and are valid without limitations.
In order to comply with the limitations of the TCM's engine performance model, it must be ensured that the total thrust neither exceeds the maximum available thrust T_{max} nor undershoots the idle thrust T_{min}. Therefore, the pseudo control input $\tilde{T}$, given by eq. (15) or (27), is compared to T_{max} and T_{min}. If $\tilde{T}$ is within its permitted range, a limitation is not required to maintain the power limits of the engine so that $\tilde{T}$ directly becomes a system input. If, on the other hand, $\tilde{T}$ is outside the power limits of the engine, the pseudo control has to be limited in order to become a valid system input. Here, the two cases $\tilde{T} > T_{max}$ and $\tilde{T} < T_{min}$ are possible scenarios which are discussed in more detail in the following.

If, in the first case, the pseudo control $\tilde{T}$ exceeds the maximum available thrust T_{max}, the pseudo controls $\tilde{V}$ and $\tilde{\dot{h}}$ have to be limited in such a way that the corresponding total thrust force T equals the maximum available thrust T_{max} so that both pseudo controls are transformed to valid system inputs $\dot{V}$, $\dot{h}$. In order to find an adequate limitation algorithm, a distinction of subcases has to be considered. For the first subcase, let $\tilde{\dot{h}}$, which is given by eq. (16) or (25), and $\tilde{V}$, which is given by eq. (17) or (22), are positive, then both pseudo controls are scaled by an identical factor to become valid system inputs ([42]). This factor is chosen in such a way that the resulting thrust, and valid system input T, is equal to the maximum available thrust T_{max} based on the TCM's engine performance database.

$$\dot{h} = \frac{T_{max} - D}{\tilde{T} - D} \cdot \tilde{\dot{h}} \tag{29}$$

$$\dot{V} = \frac{T_{max} - D}{\tilde{T} - D} \cdot \tilde{V} \tag{30}$$

For the second subcase, let $\tilde{\dot{h}}$, which is given by eq. (16) or (25), be negative and $\tilde{V}$, which is given by eq. (17) or (22), are positive, then the excessive thrust is due to the aircraft's absolute acceleration. Therefore, the aircraft's ROCD is kept so that the pseudo control $\tilde{\dot{h}}$ becomes a valid system input $\dot{h}$ and the aircraft's total acceleration is reduced in such a manner that the pseudo control $\tilde{T}$ does not exceed the maximum available thrust T_{max}:

$$\dot{V} = \frac{T_{max} - D}{m} - \frac{g}{V_{TAS}} \cdot \tilde{\dot{h}}. \tag{31}$$

For the third subcase, let $\tilde{V}$, which is given by eq. (17) or (22), be negative and $\tilde{\dot{h}}$, which is given by eq. (16) or (25), be positive, then the excessive thrust is due to the aircraft's ROCD. Therefore, the aircraft's absolute acceleration is kept so that the pseudo control $\tilde{V}$ becomes a valid system input $\dot{V}$ and the aircraft's ROCD is reduced in such a manner that the pseudo control $\tilde{T}$ does not exceed the maximum available thrust T_{max}:

$$\dot{h} = \left[\frac{T_{max} - D}{m} - \tilde{V}\right] \cdot \frac{V_{TAS}}{g}. \tag{32}$$

If, in the second case, the pseudo control $\tilde{T}$ undershoots the minimum available thrust T_{min}, the pseudo controls $\tilde{V}$ and $\tilde{\dot{h}}$ have to be modified in such a way that the corresponding total thrust force T equals the minimum available thrust T_{min} so that both pseudo controls are transformed to valid system inputs $\dot{V}$, $\dot{h}$. As before, the aim is to provide an adequate limitation algorithm where we have to distinguish between three different subcases ([42]). For the first subcase, let $\tilde{\dot{h}}$, which is given by eq. (16) or (25), and $\tilde{V}$, which is given by eq. (17) or (22), are negative, then both pseudo controls are scaled by an identical factor to become valid system inputs. This factor is chosen in such a way that the resulting thrust, and valid system input T, is equal to the minimum available thrust T_{min} based on TCM's engine performance database.

$$\dot{h} = \frac{T_{min} - D}{\tilde{T} - D} \cdot \tilde{\dot{h}} \tag{33}$$

$$\dot{V} = \frac{T_{min} - D}{\tilde{T} - D} \cdot \tilde{V} \tag{34}$$

For the second subcase, let $\tilde{\dot{h}}$, which is given by eq. (16) or (25), be negative and $\tilde{V}$, which is given by eq. (17) or (22), are positive, then the diminished thrust is due to the aircraft's ROCD. Therefore, the aircraft's absolute acceleration is kept so that the pseudo control $\tilde{V}$ becomes a valid system input $\dot{V}$ and the aircraft's ROCD is limited in such a manner that the pseudo control $\tilde{T}$ does not undershoot the minimum available thrust T_{min}:

$$\dot{h} = \left[\frac{T_{min} - D}{m} - \tilde{V}\right] \cdot \frac{V_{TAS}}{g}. \tag{35}$$

For the third subcase, let $\tilde{V}$, which is given by eq. (17) or (22), be negative and $\tilde{\dot{h}}$, which is given by eq. (16) or (25), be positive, then the diminished thrust is due to the aircraft's absolute acceleration. Therefore, the aircraft's ROCD is kept so that the pseudo control $\tilde{\dot{h}}$ becomes a valid system input $\dot{h}$ and the aircraft's absolute acceleration is limited in such a manner that the pseudo control $\tilde{T}$ does not undershoot the minimum available thrust T_{min}:

$$\dot{V} = \frac{T_{min} - D}{m} - \frac{g}{V_{TAS}} \cdot \tilde{\dot{h}}. \tag{36}$$

4. SIMULATION RESULTS

This section presents simulation results for the ZD and CCC flight controller embedded within TCM's closed-loop control system of STRATOFLY MR3 (see FIG. 3). As reference mission, a flight route from Brussels (geodetic latitude: $50.843°$, geodetic longitude: $1.263°$) to Sydney (geodetic latitude: $-35.896°$, geodetic longitude: $150.146°$) with a cruise Mach number of 8 and a take-off weight of 400 t is considered resulting in a total travelled distance over ground of 18 717.36 km and a flight time of approximately 193 min (3h 13 min). The initial cruise flight altitude h_{ICA} is set to 109 000 ft (33 223 m) whereas the altitude for the engine switch (from ATR to DMR, vice versa) is predefined at 77 000 ft (23 470 m) for the climb profile and at 60 000 ft (18 288 m) for the descent profile. Regarding TCM's adaptive sampling time method, a fixed sampling time increment of $\Delta t = 1\ s$ propagates the time-history simulation which is only reduced during phase transitions where higher accuracy is required.

FIG. 6 illustrates the C_l- and V_{TAS}-tracking over time for the CCC flight controller during the cruise flight segment which approximately covers a flight time from 52 to 147 min. The aircraft's lift coefficient and true airspeed are tracking their reference trajectories $C_{l,r}$ and $V_{TAS,r}$ very accurately which implies a good controller performance. For the controller set up, the feedback gains $k_{p,C_l} = 0.0112$, $k_{i,C_l} = 0.00003$, $k_{p,TAS} = 0.13$ and $k_{i,TAS} = 0.005$ are chosen constant and Hurwitz [47]. Note that, since MR3 reaches in most cases the initial cruise flight altitude with a Mach number smaller than the cruise flight Mach number (due to numeric), the first part of cruise flight segment (here from ~52 to ~59 min) represents an acceleration phase where the C_l-based lift coefficient controller is not active due to TCM`s internal calculation routine. Only after the acceleration phase, the reference trajectory $C_{l,r}$ becomes valid. Likewise, the reference trajectory $V_{TAS,r}$ becomes valid at approximately 59 min of flight time.

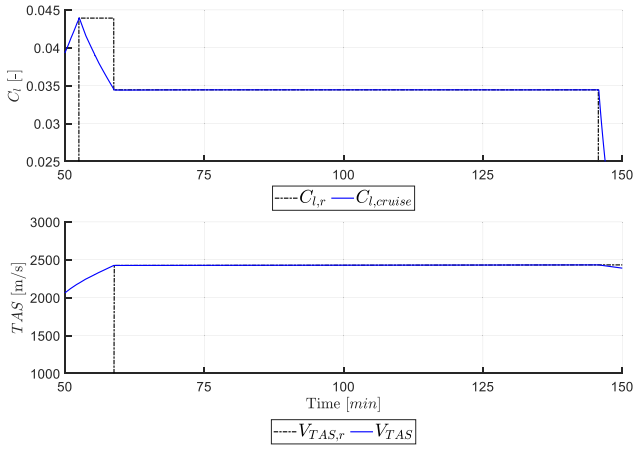

FIG. 6: Lift coefficient and true airspeed tracking over time during cruise flight segment for CCC flight controller

FIG. 7 shows the E_S-tracking over time for the ZD flight controller between the sub- and supersonic climb segment (transonic regime) which approximately covers a short-range flight time from 10.8 to 12.2 min. The aircraft's specific energy level E_S tracks its reference trajectory $E_{S,r}$ accurately which implies a good and satisfying controller performance. Here, the feedback gains $k_{p,ZD} = 0.175$ and $k_{i,ZD} = 0.003$ are chosen constant and Hurwitz [47]. Note that, since TCM's vertical flight phase table defines a Mach range from 0.95 to 1.05 as transonic regime, the ZD flight controller is only active for this speed range.

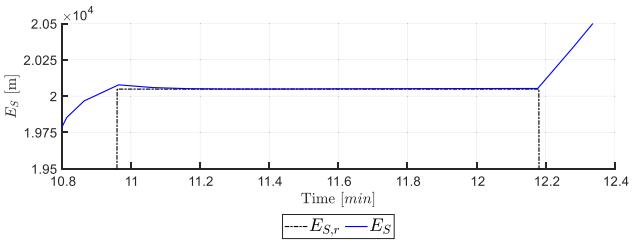

FIG. 7: Specific energy tracking over time during climb segment (transonic regime) for ZD flight controller

In comparison to a constant altitude and constant true airspeed cruise flight program, inclusion of the CCC flight controller within TCM's closed-loop control system results in a reduction of the total trip fuel consumption by 0.82% for h_{ICA} being equal to 109 000 ft (33 223 m). The total trip fuel consumption of MR3 is further reduced to an optimum of 2.64% by choosing an ICA of 98 000 ft (29 870m). With the integration of the ZD flight controller, a further trip fuel reduction of ~0.34% can be achieved which leads to a total fuel reduction of 2.98% for the fuel-optimized trajectory of MR3 resulting in a total trip fuel of 159 551 t.

5. SUMMARY, CONCLUSION AND OUTLOOK

In this paper, we presented two artificial flight controllers, the continuous climb cruise (CCC) controller as well as the zoom dive (ZD) controller, both satisfying fuel-optimized trajectories for a hypersonic vehicle concept STRATOFLY MR3. The controllers were derived using Feedback Linearization and embedded into a MATLAB-based 4D-trajectory simulation program where the vehicle dynamics are based on a 3 degrees of freedom point-mass model. Preliminary simulation results were presented proving that a fuel reduction of 2.98 % can actively be achieved by the CCC and ZD flight controllers. This results in a fuel-optimized trajectory for MR3 with a total trip fuel of 159 551 t. We pose that both controllers are advantageous to cope with the environmental strain of hypersonic air transport systems which is justified by the assumption that pollutant emissions like H_2O are approximately proportional to an aircraft's fuel flow.

Further analysis of both proposed controller architectures, however, is still required since stability or rather semi–global stability was not within the scope of this paper. Future work shall also hone the presented approach to not only derive *fuel-efficient* flight controllers (in order to calculate fuel-optimized trajectories for MR3), but also to be able to asses minimum-emissions trajectories of MR3 since time and locus of an emission are important parameters for the climate impact assessment of a new vehicle design (especially with respect to non-CO_2 effects such as NO_x emissions, water vapour or contrails).

ACKNOWLEDGMENT:

This project has received funding from the European Union's Horizon 2020 research and innovation programme under grant agreement No 769246 within the

Stratospheric Flying Opportunities for High-Speed Propulsion Concepts (STRATOFLY) Project.

REFERENCES:

[1] Viola, N., Fusaro, R., Gori, O., Marini, M., Roncioni, P., Saccone, G., Saracoglu, B., Ispir, A. C., Fureby, C., Nilsson, T., Ibron, C., Zettervall, N., Nordin Bates, K., Vincent, A., Martinez-Schram, J., Grewe, V., Pletzer, J., Hauglustaine, D., Linke, F., Bodmer, D.: STRATOFLY MR3 – how to reduce environmental impact of high-speed transportation. In: AIAA Scitech 2021 Forum, pp. 1–21. VIRTUAL EVENT (2021). https://doi.org/10.2514/6.2021-1877

[2] McClinton, C., Hunt, J., Ricketts, R., Reukauf, P., Peddie, C.: Airbreathing hypersonic technology vision vehicles and development dreams. In: 9th International Space Planes and Hypersonic Systems and Technologies Conference, pp. 1–16. Norfolk, Virginia, USA (1999). https://doi.org/10.2514/6.1999-4978

[3] McClinton, C.: X-43–Scramjet Power Breaks the Hypersonic Barrier Dryden Lectureship in Research for 2006. In: 44th AIAA Aerospace Sciences Meeting and Exhibit, pp. 1–18. Reno, Nevada, USA (2006). https://doi.org/10.2514/6.2006-1

[4] Moses, P. L., Bouchard, K. A., Vause, R. F., Pinckney, S. Z., Ferlemann, S. M., Leonard, C. P., Taylor III, L. W., Robinson, J. S., Martin, J. G., Petley, D. H., Hunt, J. L.: An airbreathing launch vehicle design with turbine-based lowspeed propulsion and dual mode scramjet high-speed propulsion. In: 9th International Space Planes and Hypersonic Systems and Technologies Conference, pp. 1–21. Norfolk, Virginia, USA (1999). https://doi.org/10.2514/6.1999-4948

[5] Steelant, J.: Sustained Hypersonic Flight in Europe: Technology Drivers for LAPCAT II. In: 16th AIAA/DLR/DGLR International Space Planes and Hypersonic Systems and Technologies Conference, pp. 1–8. Bremen, Germany (2009). https://doi.org/10.2514/6.2009-7240

[6] Viola, N., Fusaro, R., Saracoglu, B., Schram, C., Grewe, V., Martinez, J., Marini, M., Hernandez, S., Lammers, K., Vincent, A., Hauglustaine, D., Liebhardt, B., Linke, F., Fureby, C.: Main Challenges and Goals of the H2020 STRATOFLY Project. Aerotec. Missili Spaz. **100**, 95–110 (2021). https://doi.org/10.1007/s42496-021-00082-6

[7] Steelant, J., Varvill, R., Walton, C., Defoort, S., Hannemann, K., Marini, M.: Achievements Obtained for Sustained Hypersonic Flight within the LAPCAT-II project. In: 20th AIAA International Space Planes and Hypersonic Systems and Technologies Conference, pp. 1–56. Glasgow, Scotland (2015). https://doi.org/10.2514/6.2015-3677

[8] Gonçalves, P. M., Ispir, A. C., Saracoglu, B. H.: Development and optimization of a hypersonic civil aircraft propulsion plant with regenerator system. In: AIAA Propulsion and Energy 2019 Forum, pp. 1–10. Indianapolis, Indiana, USA (2019). https://doi.org/10.2514/6.2019-4421

[9] Nista, L., Saracoglu, B. H.: Numerical investigation of the STRATOFLY MR3 propulsive nozzle during supersonic to hypersonic transition. In: AIAA Propulsion and Energy 2019 Forum, pp. 1–16. Indianapolis, Indiana, USA (2019). https://doi.org/10.2514/6.2019-3843

[10] Ispir, A.C., Saracoglu, B.H.: Development of a 1D dual mode scramjet model for a hypersonic civil aircraft. In: AIAA Propulsion and Energy 2019 Forum, pp. 1–9. Indianapolis, Indiana, USA (2019). https://doi.org/10.2514/6.2019-3842

[11] Scigliano, R., Marini, M., Roncioni, P., Fusaro, R., Viola, N.: STRATOFLY High-Speed Propelled Vehicle Preliminary Aero-Thermal Design. In: International Conference on Flight Vehicles, Aerothermodynamics and Re-entry Missions and Engineering, pp. 1–12. Monopoli, Italy (2019)

[12] International Civil Aviation Organization. Annex 16 to the Convention on International Civil Aviation – Environmental Protection – Volume II: Aircraft Engine Emissions. Ed. **3**, ICAO (2008)

[13] International Civil Aviation Organization. Continuous Climb Operations (CCO) Manual –unedited advance version. DOC 9993AN/495, Ed. **1**, ICAO (2013)

[14] Dalmau, R., Prats, X.: How much fuel and time can be saved in a perfect flight trajectory? Continuous cruise climbs vs. conventional operations. In: 6th International Conference of Research in Air Transportation, pp. 1–8. Istanbul, Turkey (2014)

[15] Dalmau, R., Prats, X.: Fuel and time savings by flying continuous cruise climbs: Estimating the benefit pools for maximum range operations. Transportation Research Part D: Transport and Environment. **35**, 62–71 (2015). https://doi.org/10.1016/j.trd.2014.11.019

[16] McConnachie, D., Bonnefoy, P., Belle, A.: Investigating Benefits from Continuous Climb Operating Concepts in the National Airspace System. In: 11th USA/Europe Air Traffic Management Research and Development Seminar (ATM2015), pp. 1–8. Lisbon, Portugal (2015)

[17] Rahman, T., Hao, Z., Yongzhi, S., Younis, Y. Kenan, Z.: Trajectory Optimization of Hypersonic Vehicle Using Gauss and Legendre Pseudospectral Method. In: Applied Mechanics and Materials Vols. **110-116**, 5232–5239 (2011). https://doi.org/10.4028/www.scientific.net/AMM.110-116.5232

[18] Ping, L.: Inverse dynamics approach to trajectory optimization for an aerospace plane. In: Journal of Guidance, Control, and Dynamics 1993 **16**(4), pp. 726–732 (1993). https://doi.org/10.2514/3.21073

[19] Hargraves, C. R., Paris, S. W.: Direct Trajectory Optimization Using Nonlinear Programming and Collocation. Journal of Guidance, Control, and Dynamics 1987 **10**(4), pp. 338–342 (1987). https://doi.org/10.2514/3.20223

[20] Rutowski, E. S.: Energy Approach to the General Aircraft Performance Problem. In: Journal of the Aeronautical Sciences 1954 **21**(3), pp. 187–195 (1954). https://doi.org/10.2514/8.2956

[21] Bryson, A. E., Desai, M. N.: The energy-state approximation in performance optimization of supersonic aircraft. In: Control and Flight Dynamics Conference, pp. 1–10. Pasadena, California, USA (1968). https://doi.org/10.2514/6.1968-877

[22] Calise, A. J.: Extended Energy Management Methods for Flight Performance Optimization. In: AIAA Journal 1977 **15**(3), pp. 314–321 (1977). https://doi.org/10.2514/3.63239

[23] Schmidt, D. K., Hermann, J. A.: Use of Energy-State Analysis on a Generic Air-Breathing Hypersonic Vehicle. In: Journal of Guidance, Control, and Dynamics 1998 **21**(1), pp. 71–76 (1998). https://doi.org/10.2514/2.4199

[24] Carter, P. H., Pines, D. J., vonEggers Rudd, L.: Approximate Performance of Periodic Hypersonic Cruise Trajectories for Global Reach. In: IBM Journal of Research and Development. **44**(5), pp. 703–714 (2000). https://doi.org/10.1147/rd.445.0703

[25] Chen, R. H., Williamson, W. R., Speyer, J. L., Youssef, H., Chowdhry, R.: Optimization and Implementation of Periodic Cruise for a Hypersonic Vehicle. In: Journal of Guidance, Control, and Dynamics 2006 **29**(5), pp. 1032–1040 (2006). https://doi.org/10.2514/1.19361

[26] vonEggers Rudd, L., Pines, D. J., Carter, P. H.: Suboptimal Damped Periodic Cruise Trajectories for Hypersonic Flight. In: Journal of Aircraft 1999 **36**(2), pp. 405–412 (1999). https://doi.org/10.2514/2.2445

[27] Wang, W., Hou, Z., Shan, S., Chen, L.: Optimal Periodic Control of Hypersonic Cruise Vehicle: Trajectory Features. In: IEEE Access, vol. **7**, pp. 3406–3421 (2018). https://doi.org/10.1109/ACCESS.2018.2885597

[28] Filippone, A.: Flight Performance of Fixed and Rotary Wing Aircraft. Elsevier (2006)

[29] Corban, J. E., Calise, A. J., Flandro, G. A.: Rapid near-optimal aerospace plane trajectory generation and guidance. In: Journal of Guidance, Control, and Dynamics 1991 **14**(6), pp. 1181–1190 (1991). https://doi.org/10.2514/3.20773

[30] Corban, J. E., Calise, A. J., Flandro, G. A.: Trajectory optimization and guidance law development for transatmospheric vehicles. In: Proceedings. ICCON IEEE International Conference on Control and Applications, pp. 1–6. Jerusalem, Israel (1989). https://doi.org/10.1109/ICCON.1989.770559

[31] Parker, J., Serrani, A., Yurkovich, S., Bolender, M., Doman,

D.: Approximate Feedback Linearization of an Air-Breathing Hypersonic Vehicle. In: AIAA Guidance, Navigation, and Control Conference and Exhibit, pp. 1–16. Keystone, Colorado, USA (2006). https://doi.org/10.2514/6.2006-6556

[32] Wu, S.-F., Guo, S.-F.: Optimum flight trajectory guidance based on total energy control of aircraft. In: Journal of Guidance, Control, and Dynamics 1994 **17**(2), pp. 291–296 (1994). https://doi.org/10.2514/3.21196

[33] Warren, A.: Application of total energy control for high-performance aircraft vertical transitions. In: Journal of Guidance, Control, and Dynamics 1991 **14**(2), pp. 447–452 (1991). https://doi.org/10.2514/3.20658

[34] Linke, F.: Environmental Analysis of Operational Air Transportation Concepts. PhD thesis, Technical University of Hamburg (2016)

[35] Bodmer, D.: Trade-Offs and Trajectory Optimization – Interim Report, GA-769246 STRATOFLY, Technical University of Hamburg (2020)

[36] Nista, L., Saracoglu, B. H.: Numerical investigation of the STRATOFLY MR3 propulsive nozzle during supersonic to hypersonic transition. In: AIAA Propulsion and Energy 2019 Forum, pp. 1–16. Indianapolis, Indiana, USA (2019). https://doi.org/10.2514/6.2019-3843

[37] Ispir, A. C., Saracoglu, B. H.: Development of a 1D dual mode scramjet model for a hypersonic civil aircraft. In: AIAA Propulsion and Energy 2019 Forum, pp. 1–9. Indianapolis, Indiana, USA (2019). https://doi.org/10.2514/6.2019-3842

[38] Goncalves P. M., Ispir A. C., Saracoglu B. H., Development and optimization of a hypersonic civil aircraft propulsion plant with regenerator system. In: AIAA Propulsion and Energy 2019 Forum, pp. 1–10. Indianapolis, Indiana, USA (2019). https://doi.org/10.2514/6.2019-4421

[39] Alligier, R., Gianazza, D., Durand, N.: Energy Rate Prediction Using an Equivalent Thrust Setting Profile. In: 5th International Conference on Research and Air Transportation, pp. 1–7, Berkeley, California, USA (2012)

[40] Stevens, B. L., Lewis, F. L.: Aircraft control and simulation. Wiley, New York (1992)

[41] Linke, F.: Trajectory Calculation Module (TCM) - Tool Description and Validation. Internal Report IB-328-2009-01, German Aerospace Center, Air Transportation Systems, Hamburg (2009)

[42] Lührs, B., Linke, F., Gollnick, V.: Erweiterung eines Trajektorienrechners zur Nutzung meteorologischer Daten für die Optimierung von Flugzeugtrajektorien. In: 63. Deutscher Luft- und Raumfahrtkongress 2014 (DLRK), pp. 1–12, Augsburg, Germany (2014). https://elib.dlr.de/90935/

[43] Sadraey, M.: Unmanned Aircraft Design: A Review of Fundamentals. Morgan & Claypool (2017)

[44] Slotine, J.-J. E., Li, W.: Applied nonlinear control. Prentice Hall, Englewood Cliffs (1991)

[45] International Organization for Standardization: The Standard Atmosphere. DIN ISO 2533. Geneva, Switzerland (1975)

[46] Lunze, J.: Regelungstechnik 1. Springer, Berlin (2010)

[47] Khalil, H.K.: Nonlinear systems, 3rd edn. Prentice Hall, Upper Saddle River (2002)